TEMPERATURE EFFECTS ON DUAL-SPACED THERMAL NEUTRON LOGGING TOOLS

by
M. P. Smith

Halliburton Logging Services, Inc.
Houston, Texas

QQ

ABSTRACT

Dual-spaced thermal neutron logs must be corrected for elevated temperatures. If this is not done, porosity readings can be pessimistic, causing reserves to be underestimated or gas presence to be erroneously indicated. These temperature corrections are not caused by electronic tool drift, but rather are the result of decreases in fluid density, nuclear cross sections, and relative detector counting efficiencies as formation temperature increases. The range of one logging tool's temperature corrections has been extended out to 500°F. Although the resulting temperature corrections can be very large, they are often significantly counterbalanced by pressure corrections. Temperature corrections find applications in deep, hot targets; in geothermal areas; in steam floods; and in zones that are underpressured.

INTRODUCTION

Environmental correction of logs has become an important part of formation evaluation, reservoir description, and reserve calculations. Recent published experimental and theoretical data have indicated that the formation temperature correction for dual-spaced thermal neutron porosity logs is very large.[1] For example, at a temperature of 300°F, a 30% porosity limestone formation would have an (uncorrected) apparent porosity approaching only 21%.[1] Thus, if no temperature correction is made, neutron porosities can appear pessimistic. Since density logs are generally much less affected by temperature, neutron-density logs at elevated temperatures can erroneously indicate gas: a typical "hourglass" crossover would not occur; instead, the neutron log would appear suppressed and a smaller crossover would result.

Fortunately, the neutron temperature correction is usually balanced by the formation pressure correction. However, under conditions of high temperatures and low pressures, a large net temperature correction can be required; this can occur in very deep formations, geothermal areas, or steam floods.

One of the main purposes of this paper is to extend the range of the dual-spaced thermal neutron temperature correction out to 500°F. Present corrections only go out to 300°F. These corrections are based on experiments with a logging tool out to about 200°F; such measurements in test tanks much beyond 200°F are beset with many technical problems and safety considerations. This paper presents an alternative method that combines laboratory data developed by the nuclear reactor industry for pure water out to 564°F with a tool model which has been used to accurately fit test tank data and predict tool responses in many other earth formations.[2,3]

One advantage of this method is that the physical mechanisms responsible for the formation temperature correction are revealed. These corrections do not arise from electronic drift of the logging tool. Instead, they are caused by decreases in fluid density, nuclear cross sections, and detector efficiencies as temperature increases.

ELECTRONIC DRIFT

Dual-spaced thermal neutron logging tools usually contain two He^3 neutron detectors that are spaced near and far from a source of fast neutrons. These detectors require considerable analog and digital circuitry to amplify and process the small signals produced by the neutron absorption reactions in the He^3 gas. One of the primary tasks of service company electrical engineers is to minimize the drift of these circuits with temperature. As the temperature varies from 20 to 200°C, the apparent drift in near to far ratio can be held to a tolerance of ± 2% on a routine basis. Electronic drift is not the source of the temperature corrections discussed in this paper.

FLUID DENSITY EFFECTS

The ratio response of a dual-spaced thermal neutron logging tool is strongly influenced by the hydrogen content of earth formations. Large near/far ratios correspond to highly porous fluid-filled formations that are rich in hydrogen. Thus, as the temperature increases, fluid density decreases, hydrogen content decreases, and apparent porosity decreases. Detailed calculations show that about 50% of the difference between true and apparent porosity is caused by this decrease in fluid density with temperature. Figure 1 shows the density of fresh water as a function of temperature, assuming a minimal confining pressure to maintain the liquid phase. For example, the density of water at 564°F is 0.723 g/cc.[4] Out to 500°F, temperature variations in the density of minerals like limestone, sandstone, and dolomite have a negligible effect on neutron response.

More formally, the neutron macroscopic cross sections for scattering and absorption are proportional to fluid density; this is true for all neutron energies. These cross sections are in turn used to compute the neutron characteristic lengths Ls, Le, L, and M*. (See definitions and equations A5 - A8 in the Appendix.) Finally, the characteristic length M* is used with direct ratio computations[2,3] to compute actual tool ratios and porosity values. Thus, the effects of density variations with temperature can be taken into account.

Since even the slowing down length Ls depends on fluid density, epithermal neutron porosity tools will also show a significant temperature effect.

The direct ratio computation model[2,3] cannot accurately predict fluid (or mineral) densities at any temperature. Instead we simply use density values based on laboratory experiments or equations of state calculations for the fluids actually present in earth formations and hydrocarbon reservoirs. The following expansion (T in degrees F) can be used whenever more accurate data is unavailable:

$$\rho_{H2O} = 1.011021 - (0.142663E{-}3)T - (0.4584425E{-}6)T^2 - (0.35015501E{-}9)T^3 \quad (1)$$

NUCLEAR CROSS SECTION TEMPERATURE EFFECTS

The second most significant factor that determines tool response as temperature varies is the explicit dependence of the microscopic nuclear cross sections on temperature, both for scattering and absorption. (See σ_s and σ_a in equations A7 and A8 in the Appendix.) Detailed calculations show that, for freshwater, about 30% of the difference between true and apparent porosity is due to this mechanism. Following a number of workers[5-9], σ_s and σ_a are written as functions of T by the equations

$$\sigma_s = \sigma_{so}\,\theta^{-m_s} \quad \text{and} \quad \sigma_a = \sigma_{ao}\,\theta^{-m_a} \quad (2)$$

where

$$\theta = \frac{T}{T_o} \quad (3)$$

with T and T_o measured in degrees K. σ_{so} and σ_{ao} are measured at T_o = 20.4°C, the standard reference temperature, with most probable energy 0.0253 eV and most probable speed 2200 m/sec. The absorption exponent m_a has the standard value of 0.500. The scattering exponent m_s has empirical values that range from 0.47 to 0.455 for freshwater; we have used the average value of 0.463 in our calculations. Values of m_s from 0.0 to 1.1 have been reported by Yurova for various other fluids containing hydrogen, carbon, and oxygen.[9] This implies m_s depends on chemical environment.

The AmBe source energy of 4.6MeV corresponds to a temperature of about 54 billion °K. Even the indium energy of 1.46 eV corresponds to a temperature of 17,000 °K. However the thermal equilibrium energy corresponding to room temperature at 75°F is only 0.025 eV. Therefore only the thermal and near thermal microscopic neutron cross sections need to be corrected for elevated temperatures.

COMPARISON OF EXPERIMENTAL AND THEORETICAL DIFFUSION LENGTHS

Combining fluid density and nuclear cross section variations with temperature allows computation of the characteristic lengths Ls, L, and M* for freshwater filled formations. There exists a large body of data obtained in the 1960's by the nuclear reactor industry on the variation of the thermal diffusion length L with temperature for water, carbon, and other materials.[7] This affords the opportunity for comparing calculated and measured values of L at elevated temperatures. Table 1, taken from the work of Rockey and Skolnik[4], indicates an excellent comparison. Figure 2 shows a further comparison between computed values of L (solid curve) and many other workers of that era.[7] By allowing fluid density and the microscopic cross sections to vary with temperature, the model is able to compute L as a function of temperature out to 564°F very accurately. As T varies from 75 to 564°F, L changes from 2.80 to 5.36 cm, a very significant change.

CHANGES IN NEAR/FAR DETECTOR EFFICIENCY WITH TEMPERATURE

Before actual tool ratios and porosity values can be computed, a third feature concerning temperature must be accounted for. Mathis[10] has very recently computed the effects due to changes in the near and far detectors' counting efficiencies as functions of filling pressure, diameter, and temperature. Detailed calculations for the DSN-II* logging tool show that about 20% of the total decrease from true porosity to apparent porosity as temperature increases is due to this effect. Mathis took into account the Maxwell-Boltzmann distribution in energies of the neutrons and the actual counting efficiencies of both detectors by using a treatment from Beckhurts and Wirtz.[11] Mathis assumed that the neutron density at each detector remains constant as the temperature increases.

We have computed a DSN-II ratio normalization factor for temperature by two different methods and found them to be numerically equivalent. In the first method, the treatment of Mathis was adopted by making adjustments for the near detector's diameter and fill pressure. (The DSN-II far detector was already described by Mathis.) This leads directly to the data in Table 2. This ratio normalizer multiplies the final computed ratio in the direct ratio computation model, thereby correcting for the change in efficiency of the near and far detectors as the temperature increases. Figure 3 shows this same ratio normalizer versus temperature; notice that it reaches 0.90 only at 572°F for the DSN-II tool.

In the second method, only the actual counting efficiencies of the near and far detectors were considered, using equation 11.2.27 from Beckhurts and Wirtz.[10,11] This is illustrated in Figure 4, which shows a plot of efficiency versus $\Sigma_a R$, where Σ_a is the macroscopic absorption cross section of He^3 given by

$$\Sigma_a = 0.1334\, P\theta^{-1/2} \tag{4}$$

* A mark of Halliburton Logging Services, Inc.

with P the He^3 fill pressure in atmospheres. R is the detector radius measured in centimeters. $\Sigma_a R$ is the probability that a thermal neutron will be absorbed in distance R, so that it is a first estimate of detector efficiency. In Figure 4, the far detector is shown with a diameter x pressure product of 25.4 cm x atm. Two near detectors are also shown, with products 10.2 and 5.2 cm x atm. As the temperature increases from 20 to 200°C, the far detector efficiency changes from 0.924 to 0.884, a drop of 4%. For the two near detectors, the changes were from 0.698 to 0.618, a drop of 12%; and from 0.410 to 0.342, a 17% drop. Using this information, the data in Figure 3 were generated for the same far detector and two different near detectors. As mentioned above, this method gives the same numerical results as the previous method based more directly on Mathis' work. In the approximations of this latter method, σ_a is allowed to vary with temperature following equation (2).

Figures 3 and 4 show that, as Mathis has pointed out, it may be advantageous to use higher fill pressures for the short spaced detector to maintain relative counting efficiency as temperature increases. This feature is likely tool dependent. According to Mathis and Tittle (private communication) the reason why this effect has not been seen by routine manufacturing tests is that the neutrons, detector, and surrounding medium may not be in thermal equilibrium.

DSN-II CORRECTIONS FOR FORMATION TEMPERATURE

When fluid density, nuclear cross section, and detector efficiency variations with formation temperature are used with our direct ratio computation model, the data shown in Table 3 and Figures 5 and 6 result. Temperatures out to 500°F (=260°C) are supported. These charts are specific to the tool DSN-II because actual detector spacings, diameters, fill pressures, and hence counting efficiencies are used in the computations. These results are in reasonable agreement with published data based on an actual logging tool out to 200°F, as well as other theoretical calculations out to 300°F.[1]

Notice that the temperature corrections shown in Table 3 can be quite large. These corrections have important applications in deep, hot targets; in steam floods; and in under-pressured areas.

DSN-II CORRECTIONS FOR FORMATION PRESSURE

For completeness, a DSN-II pressure correction is shown in Figure 7 for freshwater. This was computed using the direct ratio computation model and assuming that the only pressure effect on the dual-spaced neutron tool is due to the increase in fluid density as the pressure is increased. The temperature remained fixed at 75°F for which the isothermal compressibility is 4.536E- 11 cm^2/dyne and the density is 0.9973 g/cc. The equivalent density increase is 0.0454 g/cc per KBAR or 0.0031308 g/cc per KPSI. Examination of Figures 6 and 7 shows that the temperature and pressure corrections have opposite signs and thereby tend to counterbalance one another.

CONCLUSIONS

Dual-spaced thermal neutron porosity tools must be corrected for formation temperature. This correction is the result of variations in fluid density, nuclear cross sections, and He^3 detector efficiency with temperature. The range of the temperature correction has been extended out to 500°F. Comparisons with nuclear reactor data at 564°F support the theoretical methods used. Although the temperature correction itself can be very large, it is often counterbalanced by the formation pressure correction.

REFERENCES

1. Gilchrist, Jr., W.A., Galford, J.E., Flaum, C., Soran, P.D., and Gardner, J.S., "Improved Environmental Corrections for Compensated Neutron Logs," SPE 15540, October, 1986.

2. Smith, M.P., "Calibration, Checking, and Physical Corrections for a Dual- Spaced Neutron Porosity Log," SPWLA Twenty-Second Annual Logging Symposium, June, 1986.

3. Smith, M.P., "Neutron Absorption Effects on Dual-Spaced Thermal Neutron Logging Tools," SPWLA Twenty-Eighth Annual Logging Symposium, June, 1987,

4. Rockey, K.S., and Skolnik, W. "Measurements on the Diffusion Length of Thermal Neutrons in Water from 25 to 296°C," Nuclear Science and Engineering, Vol.8, pp. 62-65, (1960).

5. Glasstone, S., and Edlund, M.C., The Elements of Nuclear Reactor Theory, Van Nostrand, Princeton, 1952.

6. Lamarsh, J.R., Introduction to Nuclear Reactor Theory, Addison-Wesley, U.S.A., 1966.

7. Reactor Physics Constants, United States Atomic Energy Commission, ANL-5800, Second Edition, 1963, Section 3.

8. Lloyd, R.C., Clayton, E.D., and Rickey, C.R., "Variations of Graphite Diffusion Length with Temperature," Nuclear Science and Engineering, Vol.4, pp.690-697, (1958).

9. Yurova, I.N., Polyakov, A.A., Stepanov, S.B., and Alimov, G.A., "Neutron Slowing Down in Hydrogen Bearing Media," USSR.

10. Mathis, G.L., "The Effect of Thermal Neutron Temperature Upon 3He Detector Response," IEEE-Nuclear Science Symposium, November, 1988.

11. Beckhurts, K.H., and Wirtz, K., Neutron Physics, Springer-Verlag, Berlin, 1964.

12. McKeon, D.C., and Scott, H.D., "SNUPAR - A Nuclear Parameter Code for Nuclear Geophysics Applications," Nuclear Geophysics, Vol.2, No.4, pp.215-230, 1988.

13. Tittle, C.W., "The Effect of Neutron Absorption on the Apparent Porosity of the Compensated Neutron Log," Nuclear Geophysics, Vol.1, No.4, pp.301-307, (1987).

14. Tittle, C.W., "Prediction of Compensated Neutron Response Using Neutron Macroparameters," Nuclear Geophysics, Vol.2, No.2, pp.95-103, (1988).

APPENDIX

This appendix provides some useful information about the theory behind dual-spaced neutron logging.

Dual-spaced neutron logs are a standard means for determining formation porosity. The tool has an AmBe fast neutron source, shielding material, and two thermal neutron detectors filled with He^3. Fast neutrons, starting with an energy of about 4.6 MeV, spread out and slow down by elastic scattering, approach thermal equilibrium, diffuse at thermal energy, and are absorbed by nuclei in the borehole/formation region. During the diffusion process, some neutrons are detected by either the near or the far detector and count rates are developed that become the primary logging input variables. A standard means for processing is to form the ratio of near count rate to far count rate and then to compute formation porosity from ratio measurements made in laboratory test formations and real earth formations.

Environmental corrections that are routinely applied at the wellsite in real time include a borehole diameter correction from the caliper log and a lithology correction (lime, san, dolomite) as selected by the engineer. In particular, a real-time temperature correction is generally not applied. Other operations that are routinely performed in real time include tool calibration, dead-time correction of count rates, depth alignment, and smoothing to limit the effects of statistics.

Nuclear characteristic lengths describe the spatial distribution of the neutrons as they slow down, spread out, and diffuse. Calculated mean squared distances are related to characteristic lengths by equations of the form

A1 $$\text{ave}[(\text{distance})^2] = 6^*(\text{characteristic length})^2$$

Both quantities are for specified neutron energy intervals. Important examples of nuclear characteristic lengths are:

CHARACTERISTIC LENGTH	NEUTRON ENERGY INTERVAL
slowing down length (Ls)	4.6 MeV - 1.46 eV
thermalizing length (Le)	1.46 eV - 0.025 eV
thermal diffusion length (L)	0.025 eV - 0.025 eV
total migration length (M)	4.6 MeV - 0.025 eV
effective migration length (M*)	4.6 MeV - 0.025 eV

M is related to Ls, Le, and L by the formula

A2 $$M^2 = (Ls)^2 + (Le)^2 + (L)^2$$

and M* by the similar expression

A3 $$(M^*)^2 = (Ls)^2 + (Le)^2 + (0.66L)^2$$

The factor of 0.66 adjusts L for the fact that the tool detects thermal neutrons after they begin the thermal diffusion process but before they are captured in the formation.[3] This numerical factor adjusts the relative contributions to M* from Ls and L and has important implications for absorption effects and temperature effects.

The mean distance squared ($\overline{d^2}$) a thermal neutron moves from the site where it first becomes a thermal neutron to the site where it is captured is given by

A4 $$\overline{d^2} = 6L^2$$

which is simply an example of equation A1. If L = 3 cm, then the average diffusion distance is 7.3 cm. This distance should not be confused with the total zig-zag path taken by the neutrons, which is generally much larger. For example, if the capture cross section is 22 cu, then this total path would be about 45 cm (≈ 1/0.022)!

A number of papers have been written showing how these lengths are calculated and used. It is even possible to compute the tool response using them.[2,3,13-14] QQ

It is instructive to see how the thermal diffusion length (L) is computed because it shows how density and microscopic cross sections are involved. L is calculated from

A5 $$L = \sqrt{D/\Sigma_a}$$

and

A6 $$D = \frac{1}{3[\Sigma_a + \Sigma_s(1-\bar{\mu})]}$$

where Σ_a and Σ_s are the macroscopic thermal neutron absorption and scattering cross sections and $\bar{\mu}$ is the cosine of the mean scattering angle at thermal energy. The macroscopic cross sections are in turn related to their corresponding microscopic cross sections σ_s, σ_a by

A7 $$\Sigma_a = N_o \sum \frac{\rho_j V_j}{M_j} \sum n_{ji}\sigma_{ai}$$

and

A8 $$\Sigma_s = N_o \sum \frac{\rho_j V_j}{M_j} \sum n_{ji}\sigma_{si}$$

where N_o is Avagadro's number; V_j, ρ_j, and M_j are fluid or mineral volume fractions, densities, and molecular weights; and n_{ji} is the number of atoms per molecule of each fluid or mineral in the formation.

As indicated by equations (2) and (3) of the main text, the microscopic cross sections σ_s and σ_a are functions of temperature.

Thus the macroscopic cross sections are linear functions of the volume fractions, densities, and microscopic cross sections. Of course, L is not such a linear function. Equations more complex and yet analogous to A5-A8 hold for Ls and Le; their microscopic cross sections must be evaluated at higher neutron energies. All of the characteristic lengths, as well as the tool ratio, are non-linear functions of volume fractions, densities, and nuclear cross sections.

TABLES

Table 1 Temperature dependence of thermal diffusion length of water as measured by Rockey and Skolnik in 1960 and as computed in the present work.
295°C is about 564°F.

T(°C)	ρ(g/cc)	Lexp (cm)	Lcalc (cm)
25.9	0.997	2.859 ± 0.018	2.850
122.7	0.941	3.444 ± 0.039	3.457
218.5	0.843	4.078 ± 0.064	4.283
295.3	0.723	5.362 ± 0.049	5.355

Table 2 DSN-II ratio normalization factor versus temperature.

T(°F)	Rnorm
50	1.010
75	1.000
122	0.985
212	0.965
302	0.945
399	0.930
572	0.901

Table 3 Apparent limestone porosity values for different temperatures and different true limestone porosities. All porosities are expressed as percentages.

	564	462	376	271	180	78.6	33	T(°F)
true phi								
60	22.45	28.65	37.02	44.73	51.67	59.45	62.09	
50	19.68	24.88	31.81	38.05	43.52	49.55	51.61	
45	18.05	22.73	28.96	34.53	39.34	44.58	46.39	
40	16.28	20.43	25.95	30.88	35.10	39.65	41.21	
35	14.38	18.00	22.82	27.13	30.80	34.73	36.09	
30	12.37	15.45	19.57	23.27	26.43	29.80	30.99	
25	10.29	12.83	16.23	19.32	21.99	24.85	25.88	
20	8.14	10.15	12.84	15.33	17.50	19.86	20.73	
15	5.94	7.44	9.46	11.35	13.01	14.86	15.58	
10	3.72	4.72	6.08	7.40	8.57	9.91	10.45	
5	1.50	2.01	2.73	3.47	4.16	4.97	5.32	
2	0.23	0.46	0.80	1.16	1.51	1.96	2.17	
1	-0.17	-0.03	0.19	0.47	0.67	0.98	1.14	
0	-0.57	-0.50	-0.40	-0.28	-0.15	0.04	0.13	

QQ

Table 4 Apparent porosity versus true porosity, for two different formation pressures. The temperature is 75°F. All porosity values are expressed as percentages.

TRUE	12.5 Kpsi	25.0 Kpsi
60.0	65.535	72.412
50.0	53.990	58.761
45.0	48.297	52.240
40.0	42.710	45.925
35.0	37.231	39.820
30.0	31.826	33.890
25.0	26.450	28.065
20.0	21.077	22.294
15.0	15.726	16.579
10.0	10.447	10.970
5.0	5.230	5.470
2.0	2.061	2.151
1.0	1.033	1.076
0.0	0.044	0.044

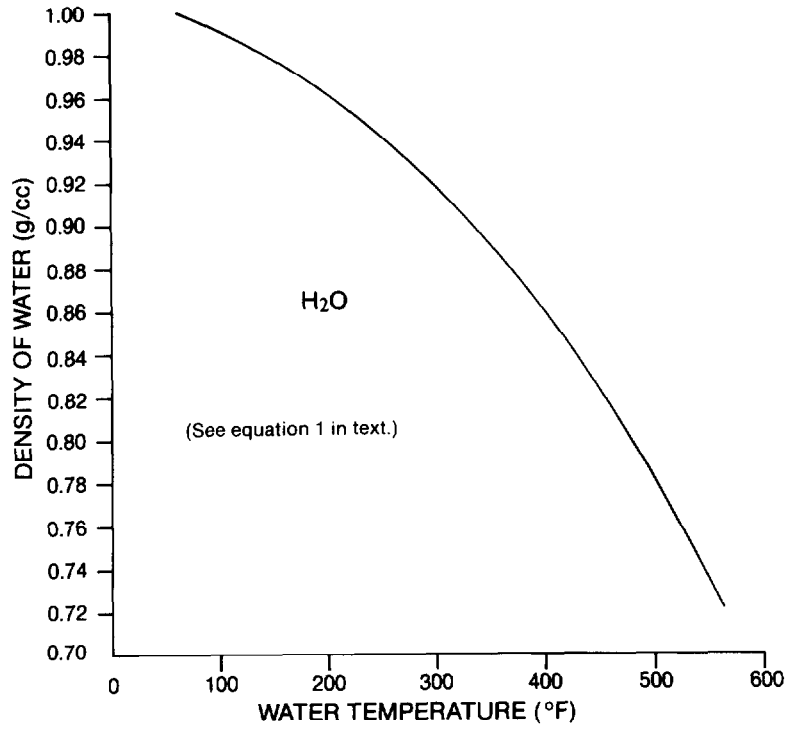

FIGURE 1. Density of water versus temperature.

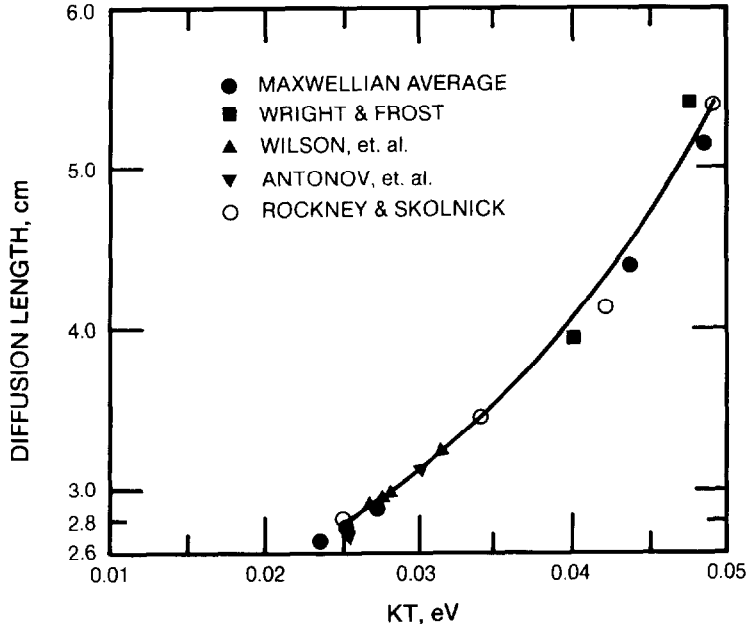

FIGURE 2. Comparison of measured and computed values of L, the thermal diffusion length of water, at elevated temperatures.

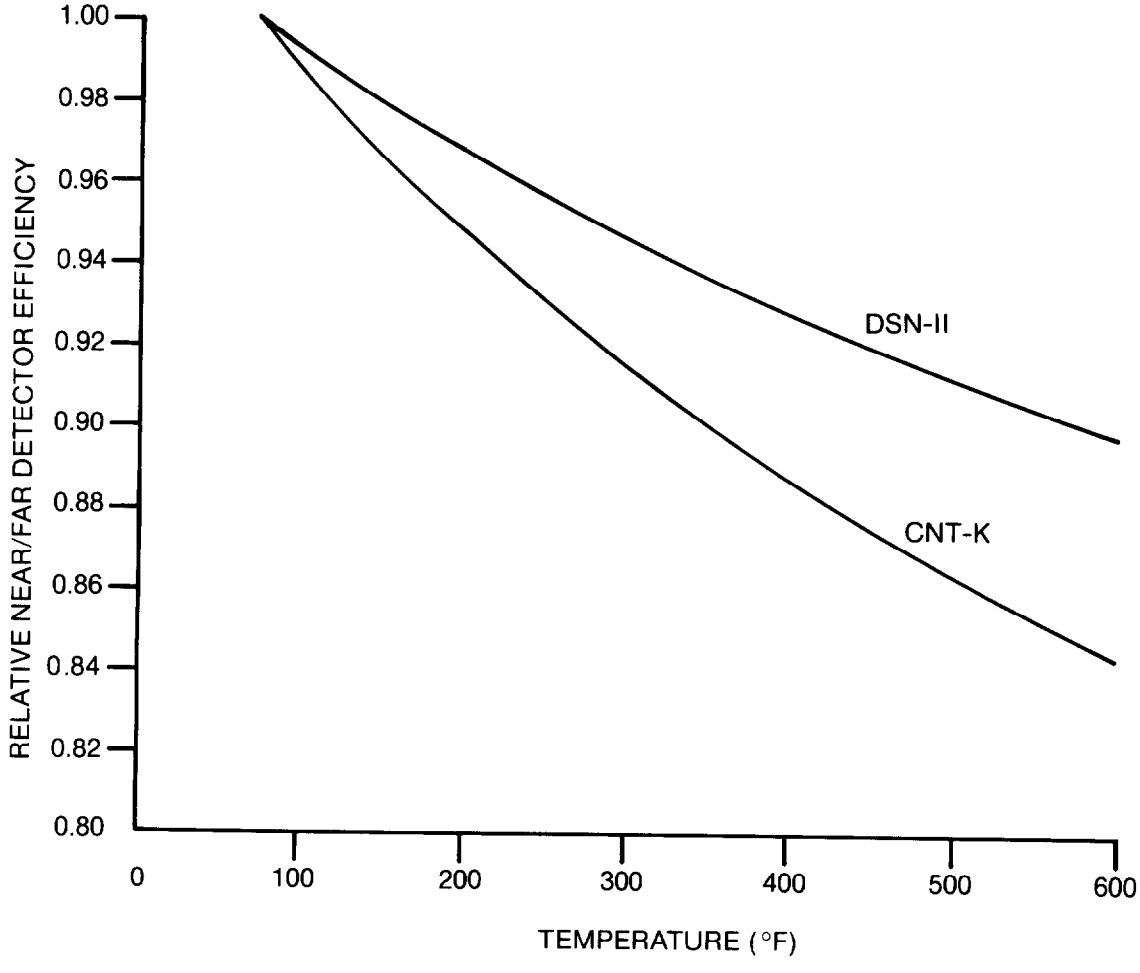

FIGURE 3. Relative near/far detector efficiency versus temperature for two different logging tools.

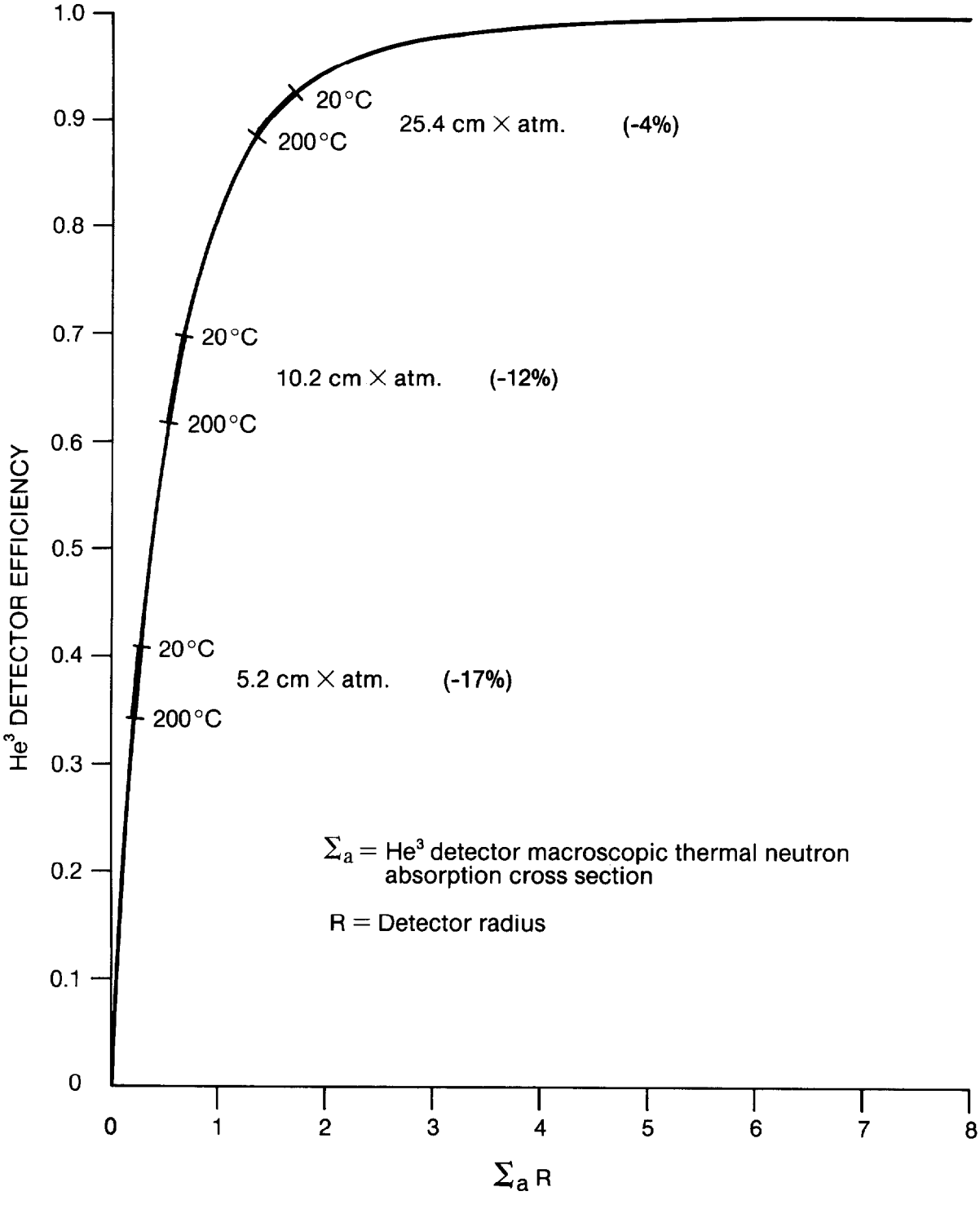

FIGURE 4. He^3 detector efficiency versus $\Sigma_a R$. See equation 11.7.27 from reference 11. One far detector is shown, together with two different near detectors.

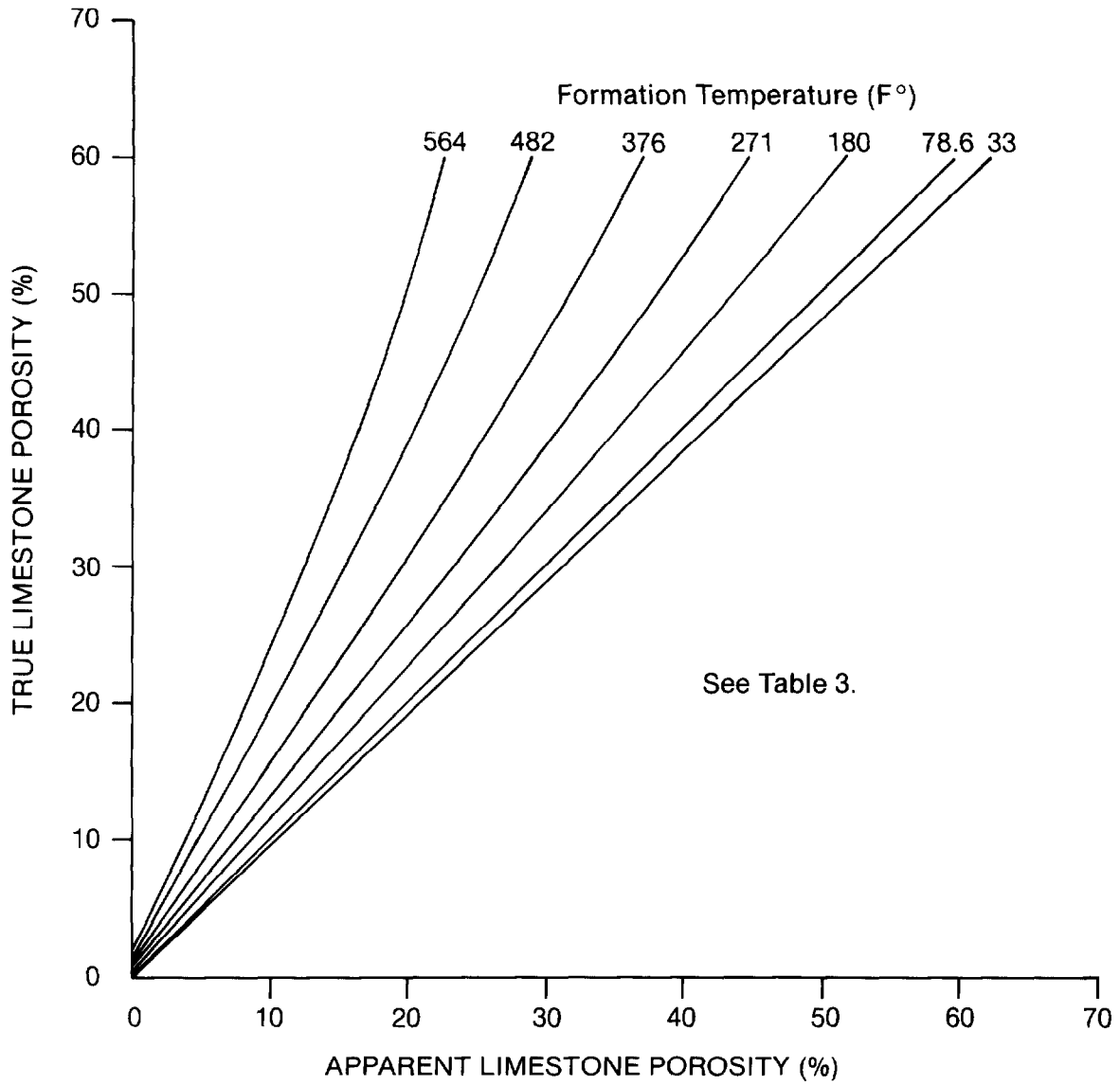

FIGURE 5. Apparent DSN-II porosity versus true porosity for temperatures from 33 to 564°F.

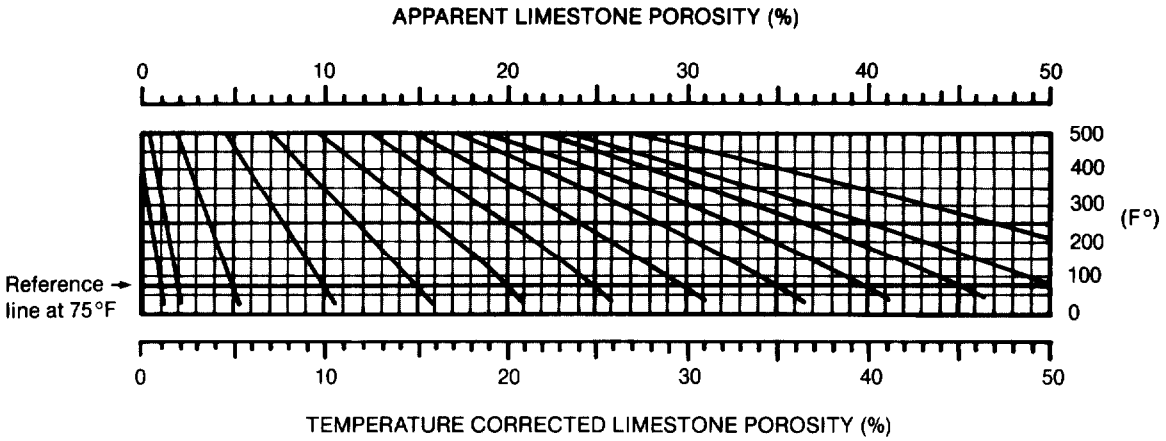

FIGURE 6. DSN-II formation temperature correction in waterfall format.

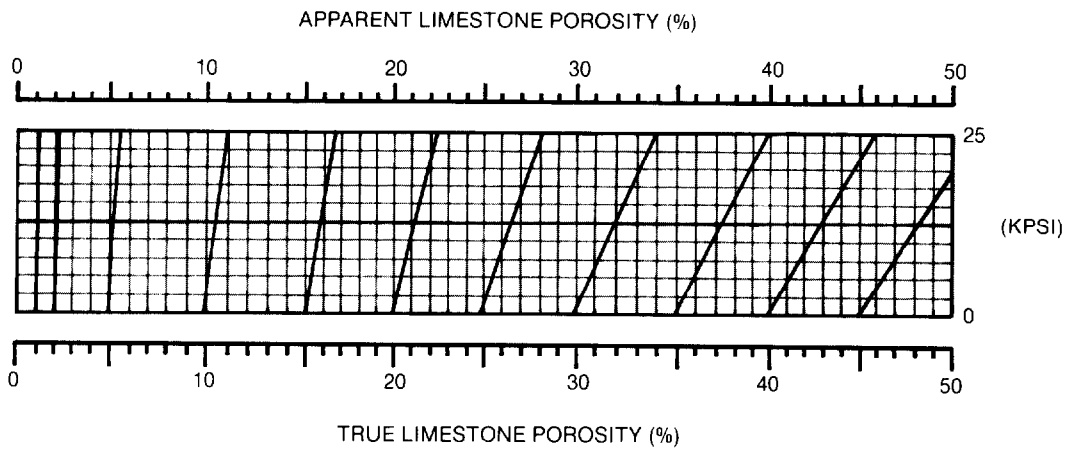

FIGURE 7. DSN-II formation pressure correction, at 75°F.

BIOGRAPHY

Michael P. Smith is a Senior Research Physicist in the nuclear group of Halliburton Logging Services. He received AB and MS degrees in physics and mathematics from Rockhurst College and The Johns Hopkins University. Mr. Smith worked for nine years at the Texaco Bellaire Research Laboratory on nuclear well logging. He has worked on computerized surface instrumentation for both Schlumberger and NL McCullough. Mr. Smith currently works on dual-spaced neutron logs and gamma ray spectroscopy. He is a member of SPWLA and has several articles and patents on well logging. Mr. Smith has been been selected as an SPWLA distinguished speaker for 1988-89.